Supporting Online Material for

Structural Topology of Phospholamban Pentamer in Lipid bilayers by a Hybrid Solution and Solid-State NMR Method

Raffaello Verardi, Lei Shi, Nathaniel J. Traaseth, Naomi Walsh, and Gianluigi Veglia*

*To whom correspondence should be addressed. vegli001@umn.edu

This file includes:

Materials and Methods

Pentameric PLN expression and purification. PLN expression and purification were carried out as previously reported (1, 2). Briefly, PLN was expressed in *E. coli* BL21(DE3) (Novagen) as a fusion protein with maltose binding protein (MBP, New England Biolabs). After amylose affinity chromatography, PLN was cleaved from MPB fusion by incubation with tobacco etch virus (TEV) protease. The final purification step was achieved by reverse phase HPLC. After lyophilization, protein masses were assessed by SDS-PAGE electrophoresis and MALDI-TOF mass spectrometry.

For U- ^{15}N and ^{13}C labeled PLN, the cells were grown in M9 minimal media containing $^{15}NH_4Cl$ (Cambridge Isotope Laboratory) and ^{13}C-glucose (Sigma-Aldrich) as the sole nitrogen and carbon sources, respectively. To label specific residues in PLN, the cells were grown in media containing all of the amino acids at natural abundance (~99.6% ^{14}N), with the exception of the amino acids of interest, which were ^{15}N labeled at the backbone amide nitrogen. For MAS experiments (DARR), the amino acids were U-^{13}C labeled. For the asymmetrically labeled sample preparations, we followed the protocol reported in Ref. (2).

For the asymmetric NOESY experiments, we utilized two different samples: one for the detection of methyl-methyl NOEs, the second for the detection amide-methyl NOEs. The first sample was obtained from mixing two different protein preparations in ^{2}H-glucose incorporating the precursors a) 2-keto-3-(methyl-$^{2}H_3$)-butyric acid-4-^{13}C, 3-$^{2}H_1$ (Leu and Val) and b) 2-ketobutyric acid-4-^{13}C, 3, 3-$^{2}H_2$ (Ile) (3). The first fusion protein was U-^{2}H with ^{13}C methyl labeling at Leu$^{\delta 1/2}$ and Val$^{\gamma 1/2}$, while the second fusion protein was U-^{2}H, with ^{13}C methyl labeling at Ile$^{\delta 1}$ only. The second sample was prepared by mixing 50% of a fusion protein U-^{2}H, ^{15}N labeled and 50% U-^{2}H with ^{13}C methyl labeled at Ile$^{\delta 1}$, Leu$^{\delta 1/2}$, and Val$^{\gamma 1/2}$. Note that the two fusion proteins were purified separately and then mixed (1:1 molar ratio) before cleavage with TEV protease to ensure uniform mixing. The mixed PLN pentamers were purified as described above. Asymmetric labeled samples for MAS-NMR experiments were prepared using the same approach. In this case, the two fusion proteins were labeled with U-^{13}C Leucine and ^{13}C Isoleucine, respectively, were mixed (1:1 molar ratio) prior to TEV cleavage and HPLC purification.

NMR sample preparation.

Solution NMR. The samples were prepared according to the procedure reported in Ref. (2). PLN was reconstituted in a phosphate buffer (120 mM Na_2HPO_4 pH 6.0, 120 mM NaCl, 3 mM NaN_3, 50mM 2-mercaptoethanol, and 5% D_2O) containing 300 mM dodecyl-phosphocoline (DPC) (Sigma-Aldrich) (or protonated DPC for the protein-DPC NOESY experiment). To avoid aggregation, all samples were denatured with 6 M guanidine-HCl and extensively dialyzed against NMR buffer prior to acquisition of the NMR spectra. For all samples, concentration of pentameric PLN was ~0.3 mM

Solid-State NMR. Mechanically oriented samples were prepared as previously described (2). First, small unilamellar vesicles in a 4:1 molar ratio of 1,2-dioleoyl-*sn*-glycero-3-phosphocholine (DOPC) and 1,2-dioleoyl-*sn*-glycero-3-phosphoethanolamine (DOPE) (Avanti Polar Lipids, Alabaster, AL). Then, we dissolved 2-4 mg of PLN in 10% SDS and added to the SUVs, followed by one freeze/thaw cycle. SDS was removed by extensive dialysis against water in the presence of 250 µM DTT. Lipid vesicles containing PLN were concentrated to ~2 mg/mL and spread onto 40 glass slides (5.7 mm × 12 mm × 0.030 mm) (Matsunami Glass Ltd, Osaka, Japan). The glass slides containing the lipid/protein preparations were incubated at 45 ºC for 3 hours, and subsequently stacked on top of each other and re-hydrated for 3-4 days in a humidity chamber (45 ºC and 99% humidity). The samples were sealed in glass cells and used for NMR measurements. For all samples, the final lipid/protein molar ratio was ~200/1. MAS samples for DARR experiments were prepared by co-dissolving 20mg of DOPC/DOPE and 1mg of ^{13}C-Leu/^{13}C-Ile PLN in organic solvent (TFE/Chloroform). The solvent was removed by evaporation under N_2 stream. The preparations were re-hydrated with 10 µL of aqueous buffer (50µM 2-mercaptoethanol, 120 mM Na_2HPO_4) and transferred into 3.2 mm zirconia thin-walled MAS rotors.

NMR experiments.

Solution NMR. For the assignment of <u>intramonomer</u> NOEs, two ^{15}N-edited NOESY spectra were acquired on a Varian spectrometer operating at 800 MHz (^{1}H Larmor frequency, NMRFAM; Madison, WI) and equipped with a cold probe. Each experiment was recorded with

512, 80, and 60 complex points in the three dimensions, with spectral widths of 9000, 9000 Hz, and 1560 Hz, respectively. The acquisition times were 57 ms, 9 ms, and 38 ms in t_3, t_2, and t_1 dimension, respectively. NOE mixing times of 90 and 220 ms were acquired with a recycle delay of 1.5 s and 8 transients for each increment. The temperature was set to 30 ºC.

For the assignment of inter-monomer NOEs, two NOESY spectra were used. The first is described in Ref. (3), whereas the second consisted of a simple ^{15}N-edited NOESY in which the ω_1-spectral window (indirect ^{1}H dimension) was reduced to 1300 Hz, resulting in aliasing of the resonances and a substantial improvement in resolution without increasing the experimental acquisition time. This was possible because of the absence ^{1}H resonances due to the deuterated background of the protein. Unambiguous assignment of the inter-monomer NOEs was achieved using chemical shift assignments of $^{13}CH_3$-Ile$^{\delta 1}$ and ^{15}NH groups. The experiment consisted of a matrix of 787, 70, and 28 complex points, and spectral widths of 10000 Hz, 4000 Hz, and 1300 Hz. The acquisition times were 79 ms, 18 ms, and 21 ms for t_3, t_2, and t_1, respectively. A mixing time of 400 ms was used with a recycle delay of 1.3 s utilizing 24 transients for each increment. The topology of the pentamer in micelles was probed by measuring NOEs between PLN and DPC (4). In this experiment PLN was labeled U-^{2}H and ^{15}N, with the detergent fully protonated. NOEs were detected using a ^{15}N-edited NOESY with 852, 60, and 30 complex points, spectral widths of 10000 Hz, 6600 Hz, and 1300 Hz and acquisition times of 85 ms, 9 ms, and 23 ms in t_3, t_2, and t_1, respectively. As with all the NOESY experiments, the mixing times were optimized using build-up curves to avoid spin diffusion. ^{1}H chemical shifts were referenced directly to 3-(trimethylsilyl)-1-propane-sulfonic acid sodium salt (Aldrich, Milwaukee, WI) at 0 ppm, whereas ^{15}N and ^{13}C were indirectly referenced (5). Complete Carbon shifts (Cα, Cβ, Co) were determined using triple resonance experiments HNCO, CBCA(CO)NH (6, 7). Secondary structure prediction (SSP) scores were obtained using the software SSP by Lewis Kay (University of Toronto: http://abragam.med.utoronto.ca/software.html.)

Solid-State NMR. Oriented solid-state NMR spectra were acquired at a 14.1 T magnetic field strength (^{1}H frequency of 600.1 MHz) using Bruker DMX (National High Magnetic Field Laboratory, NHMFL; Tallahassee, FL) and Varian VNMRS spectrometers. The 2D polarization inversion spin exchange at the magic angle (PISEMA) experiment (8) was performed at $\gamma B_1/(2\pi)$ strength of 60 kHz for the ^{1}H 90° pulse, cross-polarization, and SPINAL64 decoupling (9). Low-

E probes with a doubly tuned, low-inductance resonator built by the RF program at the NHMFL were used (10). PISEMA experiments were acquired with 4k scans and 12 t_1 increments for ^{15}N-Leu, ^{15}N-Cys, ^{15}N-Ile, and ^{15}N-Val PLN, 12k scans and 8 t_1 increments for ^{15}N-Ala, ^{15}N-Asn and ^{15}N-Arg PLN, and 20k scans and 8 t_1 increments for ^{15}N-Thr. All experiments used a recycle delay of 4 s. The spectra were processed using NMRPipe (11) and viewed with NMRVIEW software (12). An exponential window function was applied by using 100-300 Hz line broadening along the ^{15}N chemical-shift dimension (t_2). No window function was used to process the data in the indirect dipolar coupling dimension. After Fourier transformation and zero-filling, the data consisted of a total matrix size of 2k x 1k points in the direct and indirect dimensions, respectively.

Dipolar assisted rotational resonance (DARR) (13) experiments were run at a 14.1 T magnetic field strength (^{1}H frequency of 600.1 MHz) using a Varian VNMRS spectrometer equipped with a 3.2 mm bioMAS probe. The DARR mixing time was set to 200 ms and utilized a radiofrequency application to ^{1}H that corresponded to the n=1 condition (15 kHz). Experiments were acquired with 1024 scans and 50 t1 increments. Temperature was set at -25º C and the sample was spun at 8 kHz or 15 kHz (note that no differences in spectra quality were detected). The DARR experiment was repeated at 5º C. The pattern for the dipolar connectivities is identical to -25º C. The signal to noise ratio was lower for the DAAR acquired at 5º C.

Structure Calculation of Hybrid Pentamer

The structure calculations were carried out with XPLOR-NIH (v.2.23) software, using the hybrid solution and solid-state NMR methods reported in Refs. (14, 15) A target function (E_T) was formulated as a linear combination of geometrical (E_{chem}), solution NMR (E_{solNMR}), and solid-state NMR (E_{ssNMR}) terms:

$$E_T = E_{chem} + E_{solNMR} + E_{ssNMR}$$

The hybrid energy E_T function was minimized with simulated annealing protocols using combined minimization and molecular dynamics. To generate the pentamer ensemble, a five-step structure calculation protocol was used as in Figure S2.

Step 1: A hybrid monomer ensemble was generated starting from a solution-NMR ensemble. After folding the secondary structure elements, solid-state NMR restraints (CSA and DC) were included in the simulated annealing protocol, starting at a temperature of 3000 K with torsion angle dynamics. The force constants for the solid-state NMR restraints were optimized using cross-validation as described previously (16). A total of 200 monomer structures were generated.

Step 2: An initial symmetric pentamer was assembled with five monomer replicates, each of which was rotated by 72° (to avoid the clash of cytoplasmic helices) and placed at a distance of 50 Å. The pentamer was subjected to a rigid-body minimization protocol using the inter-monomer NOEs.

Step 3: Solid-state and solution NMR restraints were then combined using a high-temperature annealing protocol similar to step 1. An initial temperature of 5,000 K was used. Non-crystallographic symmetry (NCS) was used to ensure that each monomer was identical in the pentamer, imposing a force constant of 50 kcal/mol. To maintain five-fold symmetry, 832 symmetry restraints were added as NOE-like distance constraints with a force constant of 10 kcal/mol (17). Planar distance restraints (18) were added to determine an initial depth of insertion with respect to the micelle and the relative positioning between the two helical domains of PLN. The restraints were derived from a normalization of the protein-detergent NOEs intensities (Figure S5) using the following equation:

$$I_{H_2O} / (I_{DPC} + I_{H_2O})$$

where I_{H2O} is the intensity of the water cross-peak, I_{DPC} is the intensity of the protein-DPC cross peak. Since Leu7, Arg14, and Asn30 residues have the same normalized values, they were chosen to lie on the same plane.

Step 4: Starting from a temperature of 500 K and using torsion angle dynamics and Cartesian molecular dynamics, the conformer local geometries were relaxed to improve the structure quality. A full VDW potential was introduced, which resulted in better side chain packing. Twenty lowest energy conformers were selected for further structural analysis.

Step 5: To better define the depth of insertion in a realistic model membrane, one of the twenty conformers from step 4 was selected for structural refinement using MD simulations in explicit DOPC lipid bilayers. To place PLN within the membrane bilayer, we used rigid body

minimization with the Ez potential, maintaining a fixed orientation with respect to the z-axis. The potential term (Ez) is database potential for insertion of helical segments into a fictitious bilayer. The final system was then set up using CHARMM-GUI (19, 20), utilizing the PARAM27 force field with the CMAP correction (21, 22). The calculations were performed using NAMD version 2.6 (23).

The optimal number of 1,2-dioleoyl-*sn*-glycero-3-phosphocholine (DOPC) lipids per leaflet was determined using $P2_1$ periodic boundary conditions (PBC) with a tetragonal unit cell (24), where the lipids can freely equilibrate between the two layers. Starting with 176 on the bottom leaflet and 151 on the top leaflet, the number of lipids converged to 167 at the bottom leaflet (lumen) and 160 on top leaflet (cytoplasm) after 3.5 ns of equilibration. Once the number of lipids converged, the system was rebuilt following the method described by Woolf and Roux (25), with P1 tetragonal PBC (112 x 112 x 112 Å) and 327 lipids. We also included 75 K^+ and 90 Cl^- ions to model 150 mM ionic strength and to maintain the electroneutrality of the system. The overall system consisted of 140,667 atoms. The dynamics of the system were simulated as an isothermal-isobaric ensemble using 310 K and at a pressure of 1 atm. The temperature was kept constant using the Langevin dynamics algorithm and the pressure of the system was controlled anisotropically, allowing the z-axis to fluctuate independently from lipid plane X-Y, which was restrained to a constant ratio of 1:1. The electrostatic interactions were calculated using particle-mesh Ewald (PME) (26) method, while a Lennard-Jones potential used for the non-bonding interactions (feathered to zero in the range of 9 to 11 Å). Hydrogen atom covalent bonds were restrained using the RATTLE algorithm using a multiple integration time-step with 6 fs for full electrostatic evaluation and 2 fs for all other energy terms. In total, we performed 10 ns of equilibration with PLN backbone atoms harmonically restrained (using a force constant of 0.5 kcal mol^{-1} $Å^{-2}$), followed by 140 ns of unconstrained MD simulations.

Supplementary Figures

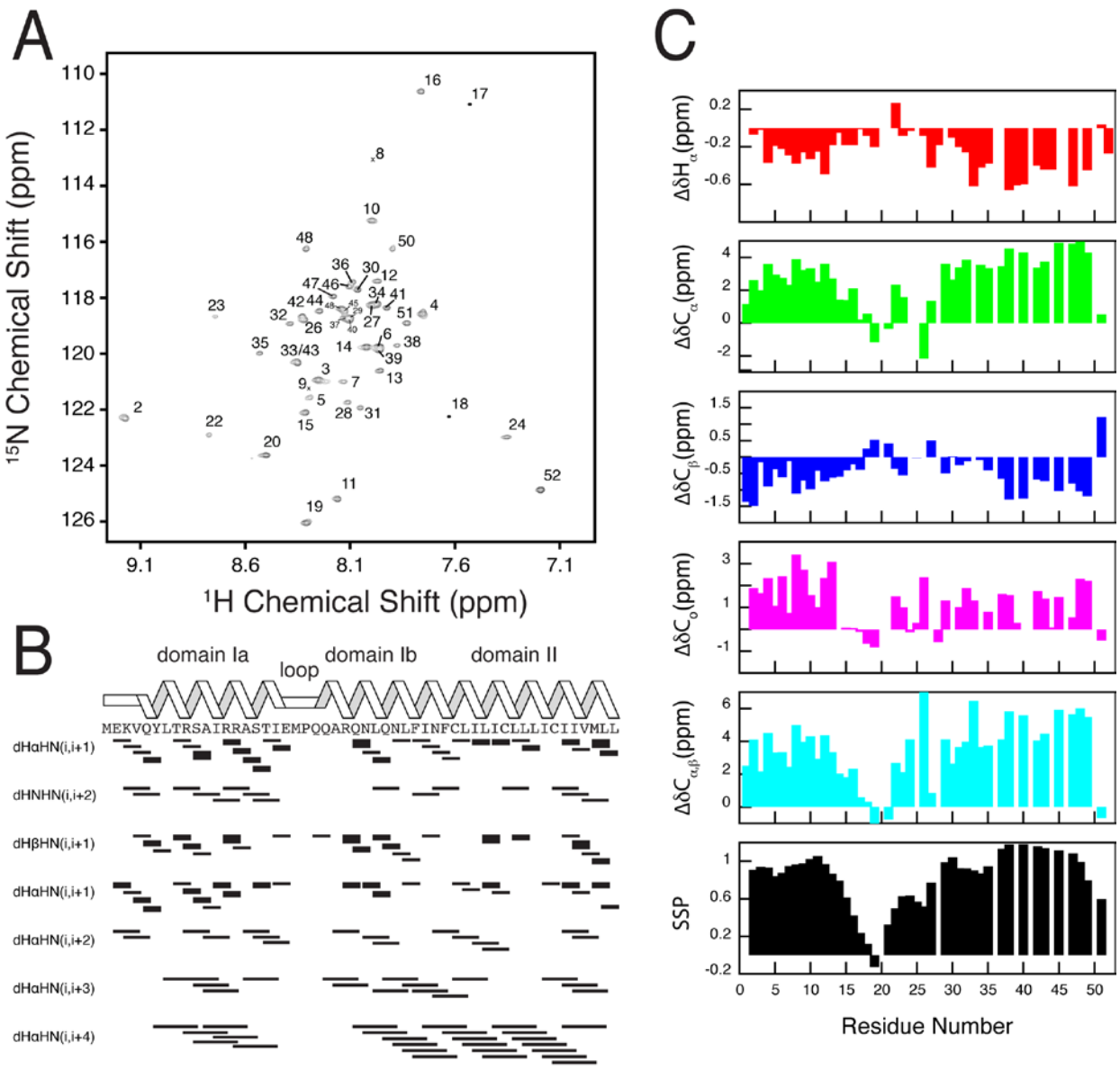

Figure S1. A) [^{1}H, ^{15}N]-TROSY HSQC spectrum of U-^{15}N labeled PLN reconstituted in 300 mM deuterated DPC. B) Plot of the short range backbone NOEs obtained from [^{1}H,^{15}N] NOESY-HSQC experiments. C) Chemical shift index histograms of PLN obtained from triple resonance experiments. Overlapping or missing residues are not shown.

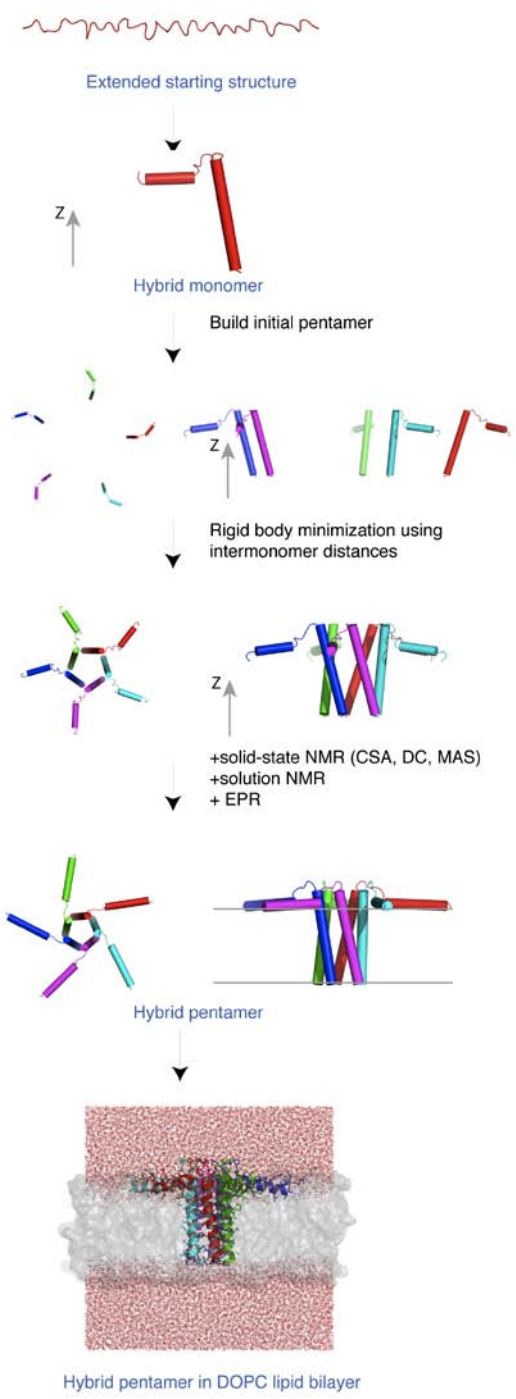

Figure S2. Overview of the hybrid refinement protocol for the simultaneous determination of structure and topology of pentameric PLN. (See SI-Methods for details).

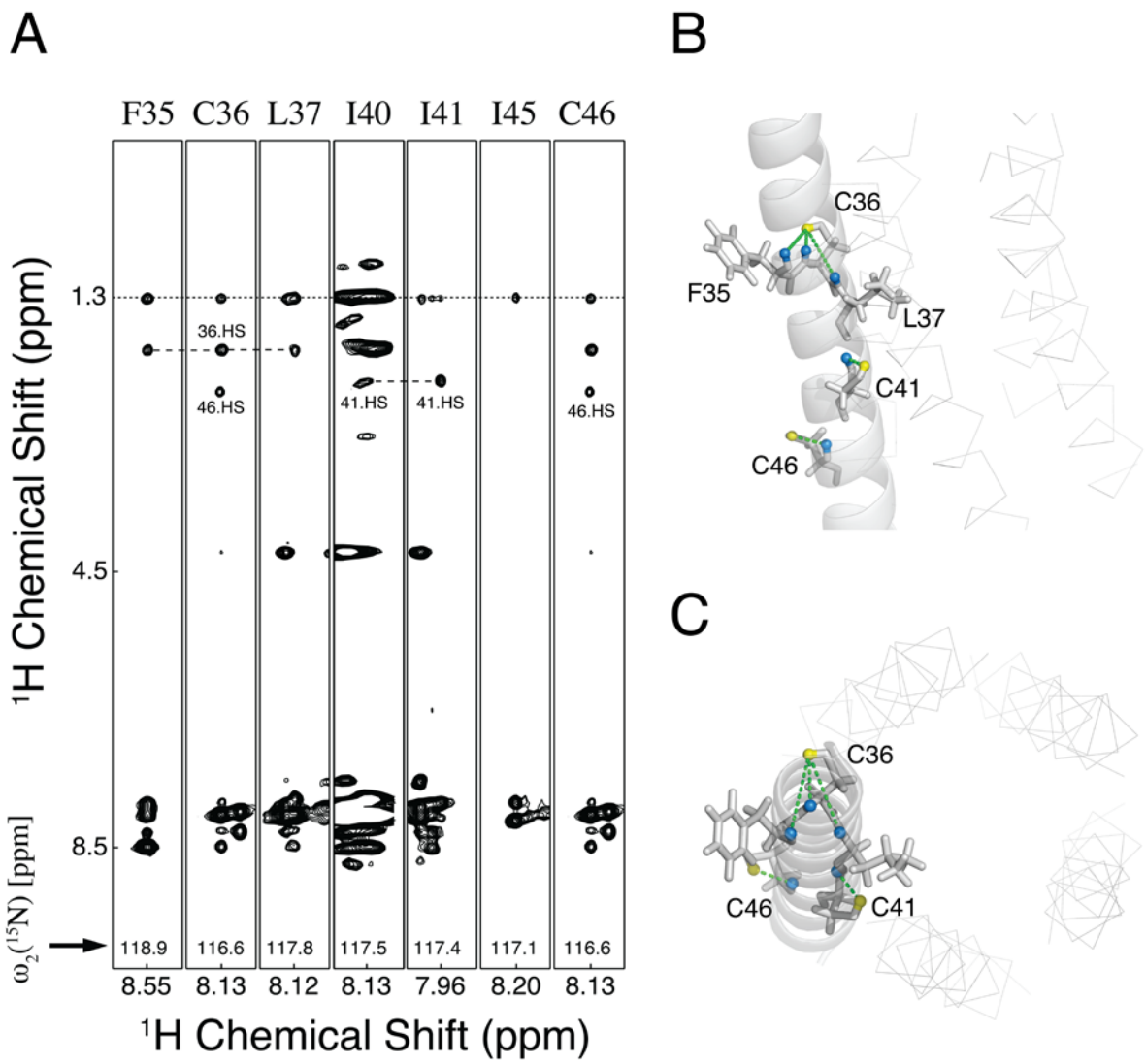

Figure S3. NOE patterns for Cys residues in PLN. A) Strip plots from a 3D ^{15}N-edited NOESY experiment on a sample of U-^{15}N PLN reconstituted in 300 mM DPC taken at the ^{15}N frequencies for specific residues. Although Cys-36 and Cys-46 have similar ^{15}N chemical shift, the residues were identified using sequential assignments. This shows that the H_γ chemical shifts are different for the three Cys residues, supporting the differential involvement in pentamer packing shown in panels B and C. Note that L37 and I40 are partially overlapped.

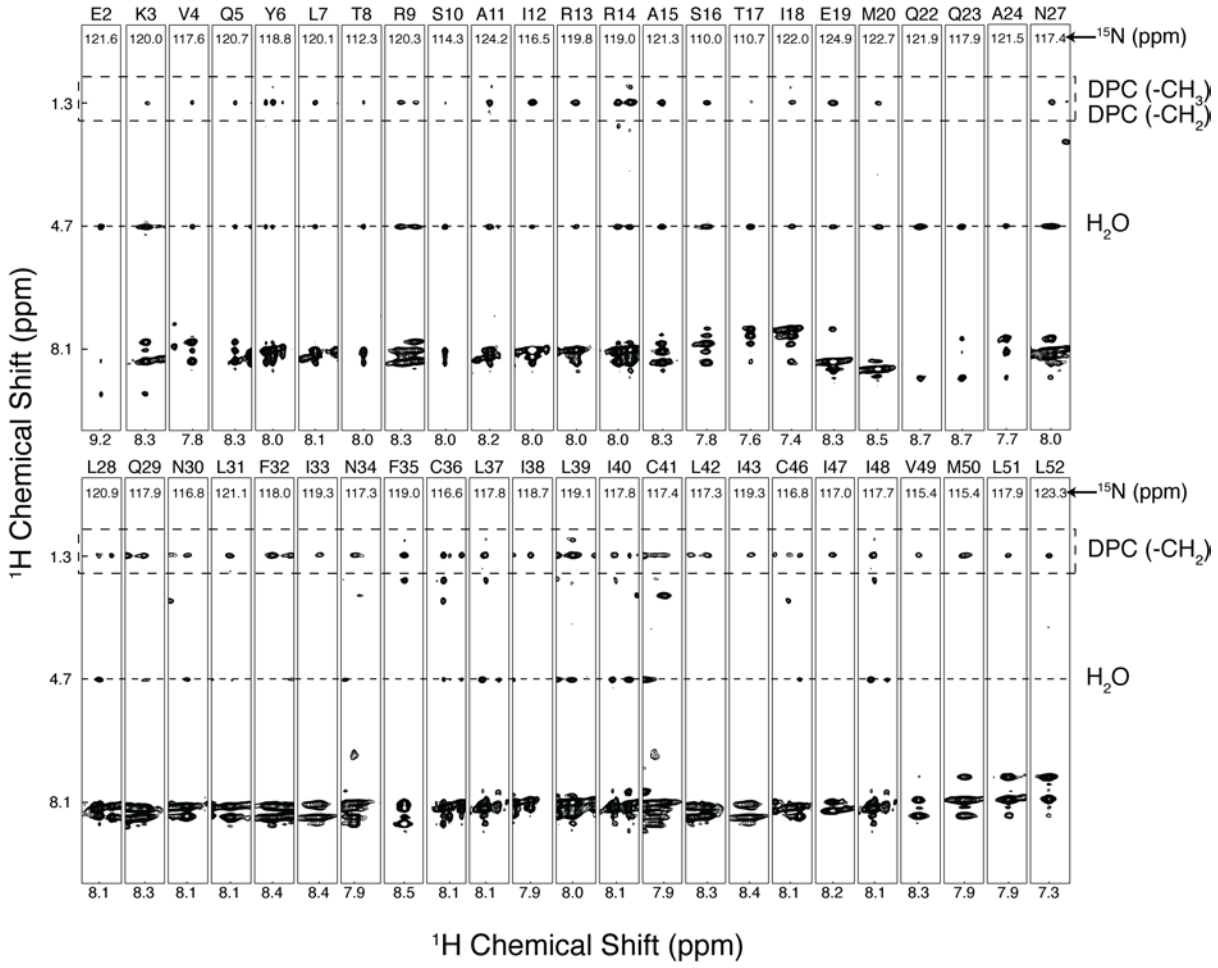

Figure S4. NOE strip plots from the ^{15}N-edited 3D NOESY of U-^{2}H, U-^{15}N PLN in protonated 300 mM DPC. Overlapping residues are not shown. The peak at 4.7ppm is assigned to the water signal and the ratios between the cross peaks and the diagonal peaks from the amide resonances was used as an indication of the water exposure of each residue (See SI methods).

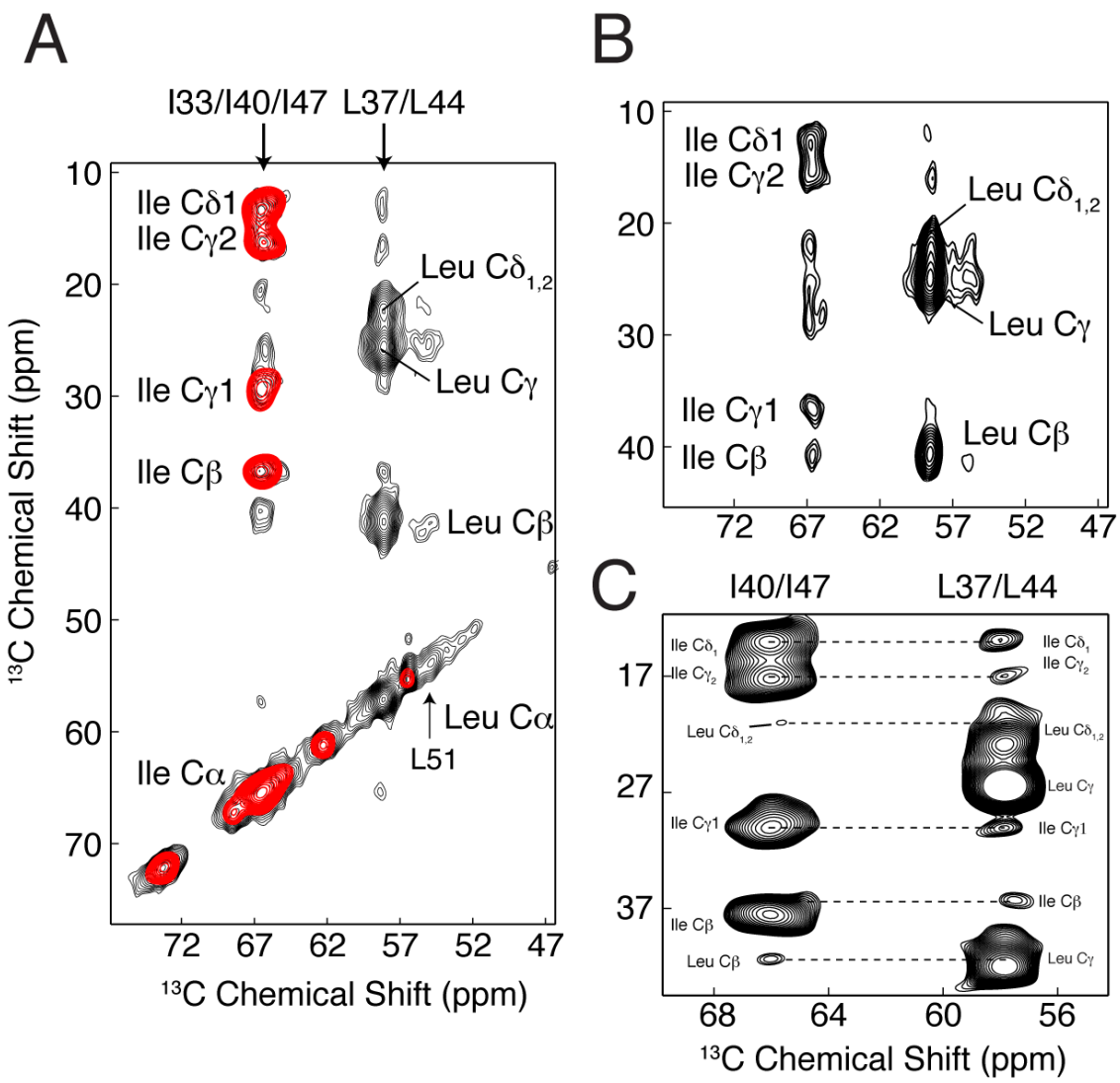

Figure S5. 2D-DARR experiments on ^{13}C-PLN samples in DOPC/DOPE lipid vesicles. A) Spectra overlay of the mixed samples with 50% U-^{13}C-Leu/ 50% U-^{13}C-Ile (black) and control sample with 100% U^{13}C-Ile PLN (red) acquired at acquired at -25ºC. Note Leu51 has a distinct chemical shift and can be unambiguously assigned based on the chemical shift found by solution NMR. B) The spectrum of the mixed sample with 50% U^{13}C-Leu/ 50% U-^{13}C-Ile PLN was acquired at 5ºC. C) The spectrum of the mixed sample of 50% U-^{13}C-Leu37/44 and 50% U-^{13}C-Ile40/47 synthesized by solid phase FMOC synthesis. The residue-specific assignments for all of the Leu and Ile residues were accomplished by acquiring 2D DARR experiments on single site 13C labeled PLN samples.

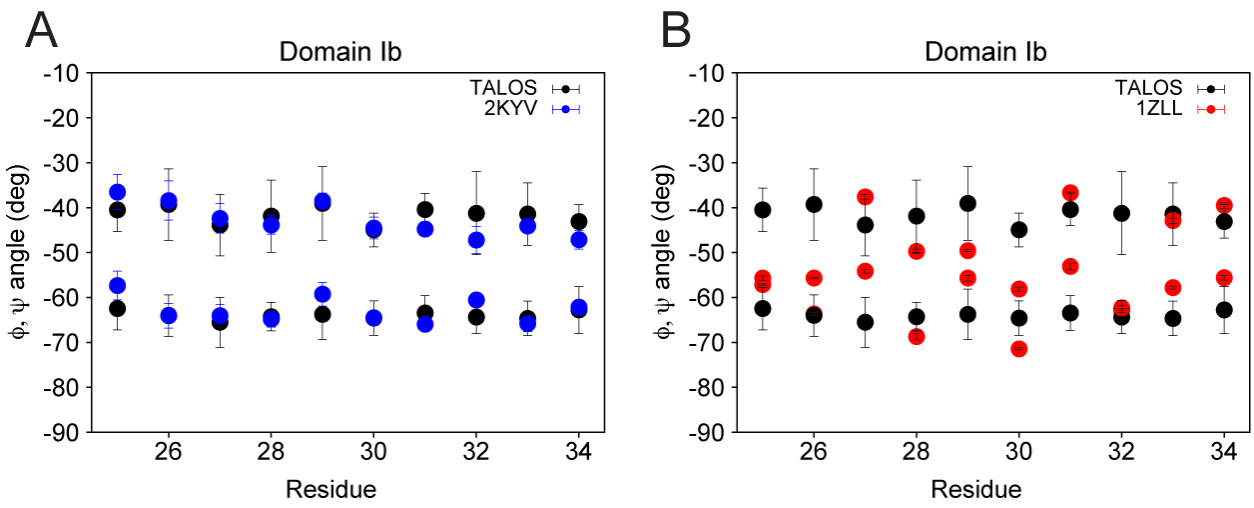

Figure S6. Agreements between the predicted dihedral angles using TALOS and the dihedral angles obtained in the calculated ensemble of the bellflower and pinwheel structural models for domain Ib (residues 25 to 34). A) Dihedral angle calculated using TALOS (27) (black) and dihedral angles back calculated from the hybrid (2KYV) ensemble (blue). B) Dihedral angle calculated using TALOS (black) and dihedral angles back calculated from the *bellflower* (1ZLL) ensemble (red).

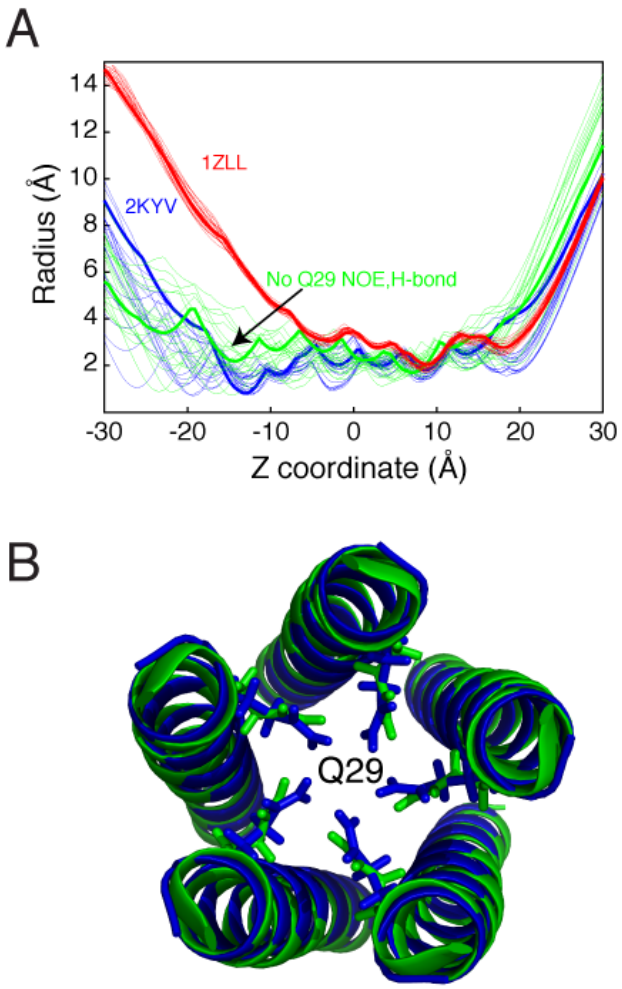

Figure S7. Effect of removing Q29 inter-monomer restraints on the packing of PLN. A) Comparison of the width of the PLN pore in the hybrid ensemble with (blue) and without (green) the Q29-Ile33 and Q29 H-bond restraints. Red traces refer to the width of the PLN pore in the *bellflower* ensemble. Thick lines correspond to the lowest energy structure in each ensemble. B) Top view of the juxtamembrane region of PLN and orientation of the Q29 side chain in the presence (blue) and absence (green) of the two intermonomer restraints.

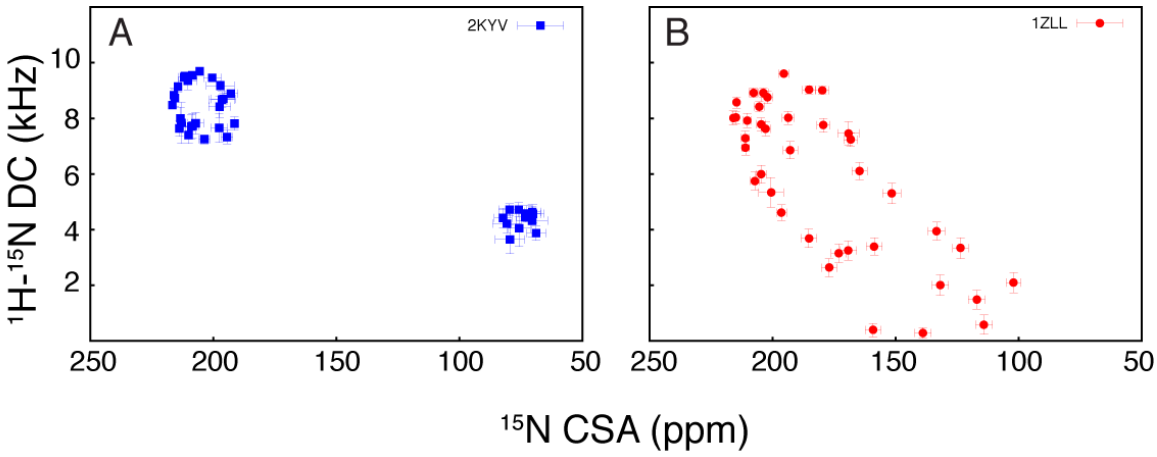

Figure S8. Comparison between PISEMA patterns back calculated from the *pinwheel* and *bellflower* ensemble. A) Back calculation of PISEMA pattern from 2KYV ensemble for residues 4-16 and 25-50. Notice the two well defined PISA wheels in the 2KYV ensemble, corresponding to domain Ia (~70ppm) and domain II (~200ppm). B) Back calculation of PISEMA pattern from 1ZLL ensemble (residues 4-16 and 25-50). The 1ZLL ensemble was aligned to one of the 2KYV PDBs using backbone atoms of residue 32 to 50

Table S1. Summary of structural ensemble statistics

RMSD from solution NMR restraints	
NOEs, Å (total: 1945 intramonomer, 75 intermonomer)	0.05 ± 0.003
Torsion angles, º (85 per monomer)	0.46 ± 0.16
PISEMA RMS	
CSA (31 per monomer, ppm)	2.8
DC (29 per monomer, kHz)	0.3
RMSD from idealized covalent geometry	
Bond, Å	0.005 ± 0.0005
Angle, º	0.6 ± 0.01
Impropers, º	0.16 ± 0.006
Measure of structural quality, % residues in	
Most Favored Region	93.9 ± 2.5
Additional Allowed Region	5.8 ± 2.2
Generously Allowed Region	0.3 ± 0.7
Disallowed Regions	0
Precision of atomic coordinates, Å	
Backbone Atoms (1-52)	4.2
Domain Ia (residues 2-18)	3.6
Domains Ib/II (residues 24-50)	0.5
Average MolProbity score[1]	1.8 (94 percentile)
Protein Topology (domain in subscript)	
$\theta_{Ia,}$ º	96 ± 3
$\rho_{Ia,}$ º	78 ± 16
$\theta_{Ib,II,}$ º	11 ± 1
$\rho_{Ib,II,}$ º	223 ± 6

[1] MolProbity scores are determined using the validation tool MolProbity (28)

Table S2. Summary of the NMR restraints from solid-state NMR

Residue	CSA (ppm)	DC (kHz)
1		
2		
3		
4	70.5	4.5
5		
6	80.2	4.5
7	66.8	4.5
8	71.0	4.1
9	72.8	4.5
10		
11	82.0	
12	65.6	4.7
13		
14	68.1	4.4
15	77.0	4.2
25	219.1	7.8
26		
27	190.6	7.9
28	216.6	6.3
29		
30	202.1	9.5
31	207.4	5.8
32	223.5	8.2
33	201.7	8.6
34	198.3	9.0
35	215.8	6.9
36	214.9	9.0
37	194.5	8.7
38		
39	220.3	6.9
40	215.8	8.9
41	193.0	
42	211.4	6.3
43	226.3	8.3
44	202.7	9.2
45	187.8	8.1
46	215.3	7.1
47	215.8	8.9
48	194.6	8.3
49	203.7	7.5
50	218.9	6.5
51		
52		

Table S3. Inter-monomer restraints (NOEs)

Monomer i	Monomer i+1	Distance (A)
Gln 29 Hε2#	Ile 33 Hδ1#	1.80 - 5.00
Ile 40 Hδ1#	Ile 40 Hδ1#	1.80 - 5.00
Ile 40 Hδ1#	Cys 41 HN	1.80 - 5.00
Leu 43 Hδ#	Ile 48 Hδ1#	1.80 - 5.00
Leu 43 Hδ#	Ile 45 Hδ1#	1.80 - 5.00
Leu 43 Hδ#	Ile 45 HN	1.80 - 5.00
Leu 43 Hδ#	Ile 45 HA	1.80 - 5.00
Leu 44 HN	Leu 44 Hδ#	1.80 - 5.00
Ile 47 Hδ1#	Leu 44 Hδ#	1.80 - 5.00
Ile 47 Hδ1#	Leu 44 Hβ#	1.80 - 5.00
Ile 47 Hδ1#	Ile 48 HN	1.80 - 5.00
Ile 47 HN	Ile 48 Hδ1#	1.80 - 5.00
Ile 47 Hδ1#	Leu 51 Hδ#	1.80 - 5.00
Ile 47 Hδ1#	Leu 52 Hδ#	1.80 - 5.00
Gln 29 Nε2	*Gln 29 Cδ*	*1.80 - 5.00**

* Distance from REDOR-NMR experiments (29)

Table S4. Experimentally measured distances in PLN

Ref.	Technique	Atom pair	Distance (Å)	Lipid System	Temp (ºC)	Hybrid
Smith *et al*. (30)	Rotational Resonance	1-^{13}C-L7/3-^{13}C-A11	4.6 ± 0.2	DMPC	-10	**4.6±0.1**
		1-^{13}C-P21/3-^{13}C-A24	4.3 ± 0.2			*6.7*±**1.3**
		1-^{13}C-L42/2-^{13}C-C46	4.7 ± 0.2			**5.0±0.1**
	REDOR	1-^{13}C-I18/$^{15}N_H$-Q22	4.7 ± 0.2			*8.3*±**0.9**
Liu W *et al.* (29)	REDOR	5-^{13}C-Q22/^{15}Ne-Q22	>5.5	POPC/POPS	-10	**16.2±2.8**
		5-^{13}C-Q26/^{15}Ne-Q26	~5.5			**5.5±1.3**
		5-^{13}C-Q29/^{15}Ne-Q29	4.1 ± 0.2***			**3.6±0.5**
Ahmed Z *et al.* (31)	Rotational Resonance	1-^{13}C-F32/2-^{13}C-A36*	4.3 ± 0.2**	DMPC	-50	**4.8±0.1**
Middleton *et al.* (32)	REDOR	1-^{15}N-L39/1-^{13}C-L37	3.2 ± 0.2	DMPC	-50	**3.2±0.02**
Hughes E and Middleton AD (33)	REDOR	2-^{13}C-A24/$^{15}N_H$-Q26	>5.0	DMPC	-40	4.2±**0.1**
	Rotational Resonance	1-^{13}C-P21/2-^{13}C-A24	4.65 ± 0.25	DMPC	-40	**6.3±1.1**
Robia *et al.* (34)	Fluorescence Energy Transfer	N-terminus/N-terminus	46.1 ± 2.1	Insect Cells microsomes	RT	**45.4±3.8**
		IA/IA	37.9 ± 3.8			**33.3±3.4**
		IB/IB	<24			**11.5±0.9**
Traaseth *et al.* (2)	DEER	Tempo-K3/Tempo-K3	47 ± 10***	DOPC/DOPE	-208	**45.0±4.9**

* In this sample Cys-36 was substituted with Alanine. ** Rotational resonance condition n=1. *** Included as restraints in the structure calculation protocol.

REFERENCES

1. Buck B, *et al* (2003) Overexpression, purification, and characterization of recombinant ca-ATPase regulators for high-resolution solution and solid-state NMR studies. *Protein Expr Purif* 30: 253-61.

2. Traaseth NJ, *et al* (2007) Spectroscopic validation of the pentameric structure of phospholamban. *Proc Natl Acad Sci U S A* 104: 14676-14681.

3. Traaseth NJ, Verardi R & Veglia G (2008) Asymmetric methyl group labeling as a probe of membrane protein homo-oligomers by NMR spectroscopy. *J Am Chem Soc* 130: 2400-2401.

4. Fernandez C, Hilty C, Wider G & Wuthrich K (2002) Lipid-protein interactions in DHPC micelles containing the integral membrane protein OmpX investigated by NMR spectroscopy. *Proc Natl Acad Sci U S A* 99: 13533-13537.

5. Wishart DS, *et al* (1995) 1H, 13C and 15N chemical shift referencing in biomolecular NMR. *J Biomol NMR* 6: 135-40.

6. Kay LE, Ikura M, Tschudin R & Bax A (1990) Three-dimensional triple-resonance NMR spectroscopy of isotopically enriched proteins. *Journal of Magnetic Resonance* 89: 496-514.

7. Grzesiek S & Bax A (1992) Correlating backbone amide and side chain resonances in larger proteins by multiple relayed triple resonance NMR. *Journal of Magnetic Resonance* 114: 6291-6293.

8. Wu CH, Ramamoorthy A & Opella SJ (1994) High-resolution heteronuclear dipolar solid-state NMR spectroscopy. *J Mag Res* 109: 270-272.

9. Fung BM, Khitrin AK & Ermolaev K (2000) An improved broadband decoupling sequence for liquid crystals and solids. *J Magn Reson* 142: 97-101.

10. Gor'kov PL, *et al* (2007) Using low-E resonators to reduce RF heating in biological samples for static solid-state NMR up to 900 MHz. *J Magn Reson* 185: 77-93.

11. Delaglio F, *et al* (1995) NMRPipe: A multidimensional spectral processing system based on UNIX pipes. *J Biomol NMR* 6: 277-293.

12. Johnson BA (2004) Using NMRView to visualize and analyze the NMR spectra of macromolecules. *Methods Mol Biol* 278: 313-352.

13. K. Takegoshi, S. Nakamura, T. Terao (2001) 13C–1H dipolar-assisted rotational resonance in magic-angle spinning NMR. *Chem Phys Lett* 344: 631.

14. Traaseth NJ, *et al* (2009) Structure and topology of monomeric phospholamban in lipid membranes determined by a hybrid solution and solid-state NMR approach. *Proc Natl Acad Sci U S A* 106: 10165-10170.

15. Shi L, *et al* (2009) A refinement protocol to determine structure, topology, and depth of insertion of membrane proteins using hybrid solution and solid-state NMR restraints. *J Biomol NMR* 44: 195-205.

16. Kim S, Quine JR & Cross TA (2001) Complete cross-validation and R-factor calculation of a solid-state NMR derived structure. *J Am Chem Soc* 123: 7292-7298.

17. O'Donoghue SI & Nilges M (1999) in *Structure computation and dynamics in protein NMR*, eds Krishna NR & Berliner LJ (Kluwer Academic/Plenum Publishers, New York, NY), pp 131-158.

18. Teriete P, Franzin CM, Choi J & Marassi FM (2007) Structure of the na,K-ATPase regulatory protein FXYD1 in micelles. *Biochemistry* 46: 6774-6783.

19. Brooks BR, *et al* (2009) CHARMM: The biomolecular simulation program. *J Comput Chem* 30: 1545-1614.

20. Jo S, Lim JB, Klauda JB & Im W (2009) CHARMM-GUI membrane builder for mixed bilayers and its application to yeast membranes. *Biophys J* 97: 50-58.

21. Mackerell AD,Jr, Feig M & Brooks CL,3rd (2004) Extending the treatment of backbone energetics in protein force fields: Limitations of gas-phase quantum mechanics in reproducing protein conformational distributions in molecular dynamics simulations. *J Comput Chem* 25: 1400-1415.

22. MacKerell AD,Jr, Feig M & Brooks CL,3rd (2004) Improved treatment of the protein backbone in empirical force fields. *J Am Chem Soc* 126: 698-699.

23. Phillips JC, *et al* (2005) Scalable molecular dynamics with NAMD. *Journal of Computational Chemistry* 26: 1781-1802.

24. Dolan EA, Venable RM, Pastor RW & Brooks BR (2002) Simulations of membranes and other interfacial systems using P2(1) and pc periodic boundary conditions. *Biophys J* 82: 2317-2325.

25. Woolf TB & Roux B (1996) Structure, energetics, and dynamics of lipid-protein interactions: A molecular dynamics study of the gramicidin A channel in a DMPC bilayer. *Proteins* 24: 92-114.

26. Darden T, York D & Pedersen L (1993) Particle mesh ewald: An N [center-dot] log(N) method for ewald sums in large systems. *J Chem Phys* 98: 10089-10092.

27. Cornilescu G, Delaglio F & Bax A (1999) Protein backbone angle restraints from searching a database for chemical shift and sequence homology. *J Biomol NMR* 13: 289-302.

28. Davis IW, *et al* (2007) MolProbity: All-atom contacts and structure validation for proteins and nucleic acids. *Nucleic Acids Res* 35: W375-83.

29. Liu W, Fei JZ, Kawakami T & Smith SO (2007) Structural constraints on the transmembrane and juxtamembrane regions of the phospholamban pentamer in membrane bilayers: Gln29 and Leu52. *Biochim Biophys Acta* 1768: 2971-2978.

30. Smith SO, Kawakami T, Liu W, Ziliox M & Aimoto S (2001) Helical structure of phospholamban in membrane bilayers. *Journal of Molecular Biology* 313: 1139-1148.

31. Ahmed Z, Reid DG, Watts A & Middleton DA (2000) A solid-state NMR study of the phospholamban transmembrane domain: Local structure and interactions with ca(2+)-ATPase. *Biochim Biophys Acta* 1468: 187-198.

32. Middleton DA, Ahmed Z, Glaubitz C & Watts A (2000) REDOR NMR on a hydrophobic peptide in oriented membranes. *J Magn Reson* 147: 366-370.

33. Hughes E & Middleton DA (2003) Solid-state NMR reveals structural changes in phospholamban accompanying the functional regulation of Ca2+-ATPase. *J Biol Chem* 278: 20835-42.

34. Robia SL, Flohr NC & Thomas DD (2005) Phospholamban pentamer quaternary conformation determined by in-gel fluorescence anisotropy. *Biochemistry* 44: 4302-4311.